In-Plane Behavior of Confined Masonry Walls –With and Without Opening

Sassan Eshghi[1,*], Khashaiar Pourazin[2]

Received:June 2008, Accepted: February 2009

Abstract: *Confined masonry buildings are used in rural and urban areas of Iran. They performed almost satisfactory during past moderate earthquakes of Iran. There is not a methodology in Iranian Seismic Code (Standard 2800-3rd edition) to estimate their capacities quantitatively. In line with removing this constraint, an attempt is made to study in-plane behavior of two squared confined masonry walls with and without opening by using a numerical approach. These walls are considered based on Iranian Seismic Code requirements. Finite element 2D models of the walls are developed and a pushover analysis is carried out. To model the non-linear behavior of the confined masonry walls, the following criteria are used: (1) The Rankine-Hill yield criterion with low orthotropic factor to model the masonry panel; (2) The Rankine yield criterion to model reinforced concrete bond-beams and tie-columns; (3) The Coulomb friction criterion with tension cutoff mode to model the interface zone between the masonry panel and reinforced concrete members. For this purpose, the unknown parameters are determined by testing of masonry and concrete samples; and by finite element analysis. Comparing the results show that the initial stiffness, the maximum lateral strength and the ductility factor of walls with and without opening are different. Also, the severe compressed zones of the masonry panels within the confining elements are found different from what are reported for the masonry panels of infilled frames by other researchers. This study shows that a further investigation is needed for estimating capacity of confined masonry walls with and without opening analytically and experimentally. Also where openings, with medium size are existed, the confining elements should be added around them. These issues can be considered in the next revisions of Iranian Seismic Code.*

Keywords: *Confined Masonry, Bond-Beams, Tie-Columns, In-Plane Behavior, Capacity Curves, Interface Modeling; Macro Modeling.*

1.Introduction

Confined masonry construction consists of unreinforced masonry walls confined with reinforced concrete (RC) tie-columns and bond-beams. This type of construction is used in urban and rural areas for low rise buildings in some earthquake prone countries in the world. As reported in the World Housing Encyclopedia [1], the following countries use confined masonry in housing construction: Slovenia, Serbia and Montenegro, Iran, Mexico, Chile, Peru, and Argentina. This type of construction seems to have strength, ductility and stiffness more than URM. If the confined masonry construction is properly constructed, it is expected to show satisfactory performance in earthquakes. Based on past studies, the most common modes of failure of confined masonry buildings [1] are: 1) shear cracks in masonry panels that propagate into the tie-columns, 2) horizontal cracks at the joints between masonry walls and reinforced concrete floors or foundations, 3) crushing of concrete at the joints between vertical tie-columns and horizontal bond-beams and 4) cracks in window piers and walls due to in-plane and/or out-of-plane action in inadequately

Fig. 1 Vertical crack in confined masonry wall due to out-of-plane action of other wall during Silakhor earthquake

* *Corresponding Author:Email: s.eshghi@iiees.ac.ir*

1 *Assistant Professor, International Institute of Earthquake Engineering and seismology.*

2 *PhD. Candidate, International Institute of Earthquake Engineering and seismology Email:pourazin@iiees.ac.ir*

confined walls (Figure 1). The unacceptable performance observed in the past earthquakes, involved houses that are built without tie-columns or bond beams, or with inadequate roof to wall connection, or with low quality materials and poor workmanship.

On the other hand, most of collapsed and damaged buildings in Iran during the past severe earthquakes were unreinforced masonry. Some of them were constructed in accordance with Iranian seismic code (i.e. they had RC bond–beams and tie–columns that confined the masonry walls). As an evidence, a confined masonry building damaged during March 31, 2006 Darbeh-Astaneh (Silakhor) earthquake is illustrated in Figure 1. The observed damage and collapse of confined masonry buildings during past earthquakes are partially due to lack of methodologies for estimating capacity of these buildings to withstand seismic loads. In Iranian seismic code (Standard No. 2800 [2]); a qualitative approach composed of series of recommendations is employed. Hence, any criterion regarding seismic performance level of new masonry buildings and/or vulnerability of existing masonry buildings can hardly be found. Therefore, these provisions are inadequate for seismic design. But in recent years, alternative seismic design approaches have been proposed in the world (e.g. NTC-M 2004, [3]) in which deformation demand and deformation capacity of confined masonry buildings can be employed.

In Mexico City Building Code requirements for masonry structures [3], the inelastic inter story drift angles of the confined masonry walls should be limited. The allowable inelastic lateral drifts are available for confined masonry walls which are derived from experimental results based on Alcocer, et al [4]. Allowable drift angles are consistent with a moderate level of damage, generally accepted in Mexico as a desirable performance of housing under the design earthquake. The allowable inelastic lateral drift angles are as follows: (1) 0.35% for confined masonry built with solid units and with horizontal reinforcement; (2) 0.25% for confined masonry built with solid units; (3) 0.25% for confined masonry built with hollow units and with horizontal reinforcement. The inelastic interstory drift angles are calculated through multiplying the elastic drift angles by the seismic behavior factor Q. The elastic drift angles obtain from analysis of the building after a reduced lateral force is applied on the building. The seismic behavior factor represents the deformation and energy dissipation capacities of the structural systems. However, in Iranian Seismic Code provisions (Standard 2800, 3rd edition), none of these issues are addressed.

The aim of this paper is to investigate the in-plane behavior of a full scale confined masonry wall with and without opening based on static nonlinear analysis. The required inelastic parameters are evaluated by a FE package DIANA(version 9.2). In another study carried out by the same authors [5], FE models are validated through experimental and analytical investigations on confined masonry wall specimens under monotonic lateral loading. A good agreement was found by comparing

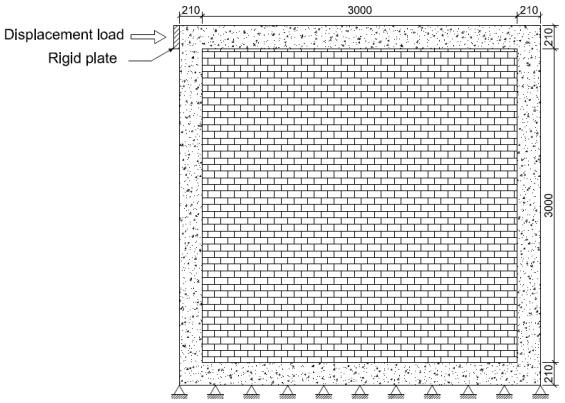

Fig. 2 The **P** wall configuration (dimensions in mm)

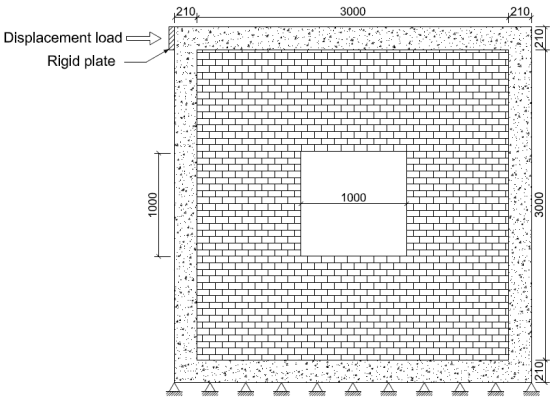

Fig. 3 The **P+O** wall configuration (dimensions in mm)

deformed shapes, crack patterns and capacity curves of these models. This study is also summarized in this paper.

2. Description of Two Models for Confined Masonry Walls

Confined masonry walls considered for in – plane analysis consist of one – story clay brick wall panel (210mm thick) confined by 210mmx210mm RC members (bond-beams and tie–columns) as shown in Figures 2 and 3. Here, two types of confined masonry walls are considered, either a panel without opening designated by (**P**), or with an opening in the center which designated by (**P+O**). The walls are assumed to be of solid fired clay bricks with dimensions 210 mm x52 mm x105mm and 10mm thick mortar joints, prepared with mortar having a volumetric ratio of 1:4 (cement : sand). The RC members are assumed to be of the concrete with a compressive strength f_c' equal to 28 MPa and 4 longitudinal reinforcement bars with 10mm diameter yielded at F_y equal to 340 MPa. Also the RC members have closed stirrups (hoops) with diameter 6 mm and F_y equal to 220 MPa. Maximum allowable hoop spacing within distance 750 mm from faces of tie-columns and/or bond beams is 150 mm center to center. Beyond distance 750 mm from the supports, maximum spacing of stirrups is 200 mm center to center. The lower RC bond – beam is restrained against the horizontal and vertical displacement but the upper one transfers static monotonic lateral displacement load.

For modeling RC bond–beams, tie–columns and masonry panel, 8 noded quadrilateral element CQ16M is used [6]. The CQ16M is a regular plane stress element (sometimes is called a membrane element) which must be thin and the loading must act in the plane of the element. For modeling interface between RC members and masonry panels, 3+3 noded CL12I line elements with zero width are used [6]. The CL12I element is an interface element between two lines in a two dimensional configuration. The configuration of combined elements is shown in Figure 4. The contact element represents a typical impenetrability constraint between adjacent bodies. This constraint defines the necessary conditions to prevent the bodies from penetrating each other [7]. However, interface elements used in this study are different from contact elements and therefore interpenetration between adjacent bodies may be occurred. Furthermore, discrete cracking may be occurred in the interface elements and thus the two interconnected bodies may be separated from each other and/or sliding at interface.

The grid pattern with mesh sizes of 200mm x55mm for RC members, 200mm x200mm for masonry wall and 200mm for interface between them are generated. Since the masonry wall is assumed as continuum, the grid size different from real brick - mortar lines may not affect the accuracy of results.

3. Material Properties of Masonry panels

The material properties used in macro-modeling of masonry panel is evaluated based on experimental studies performed in IIEES

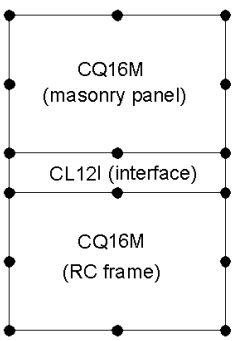

Fig. 4 Combined elements configuration

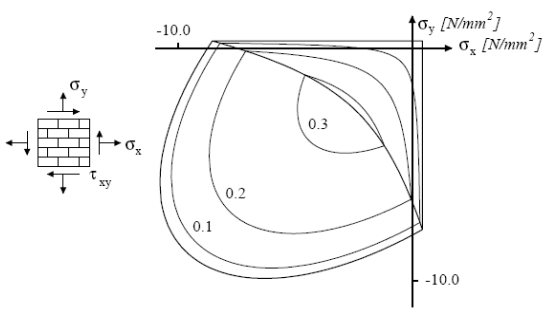

Fig. 5 Calculated composite yield criterion for solid clay brick masonry of Page (1981 , 1983), with iso-shear stress lines [8]

laboratory. In this study, a macro–modeling in which isotropic elasticity is combined with orthotropic inelastic behavior is used for modeling of masonry panel of the confined masonry wall. By using this modeling, it is anticipated that the resulted smeared cracking within the wall is well distributed and also a good agreement between experimental and numerical results would occur. In this study, the plasticity based crack model for masonry panel including a Hill type yield criterion for compression and a Rankine type yield criterion for tension which proposed by Lourenco [8] is adopted (Fig.5). The adopted material model has seven strength parameters (f_{tx} , f_{ty}, f_{mx}, f_{my}, α , β and γ) and five inelastic parameters(G_{ftx}, G_{fty}, $G_{fc.}$, G_{fcy} and κ_p). The first group of four strength parameters are the uniaxial tensile and compressive strength along the material axes *x* and *y*. The α parameter demonstrates the shear stress contribution to tensile failure. The β parameter indicates the amount of coupling between the normal stresses in the case of compressive failure. The γ parameter shows shear stress contribution to compressive failure. The second group of four inelastic parameters include fracture energies in tension and compression along *x* and *y* axes. The equivalent plastic strain κ_p , corresponding to the peak compressive strength, is the additional inelastic parameter.

Fig. 6 Cracking and failure development in masonry sample No.3 at last loading step

Based on the experimental results from Page [9], [10] on masonry samples and their related shape of the composite yield criterion, the low degree of anisotropy ($\frac{f_{tx}}{f_{ty}}$ and $\frac{f_{mx}}{f_{my}}$ are close to unity) can be achieved. This condition is occurred when the samples are built from solid clay bricks and all of the joints in masonry samples are filled with mortar. An attempt is made to reproduce test samples which are almost the same as the samples tested by Page (1981, 1983). According to Lourenco [8] deductions on his experiments, a low orthotropic factor is assumed for the samples constructed in IIEES laboratory.

In order to find the compression regime of the Rankin-Hill yield surface, three similar samples, with compression caps at both ends, are constructed in IIEES laboratory in accordance with Eurocode 6 (EN 1052-1[11]). The masonry samples have dimensions of 115x235x402, 110x245x385 and 113x243x376, all in mm. The uniaxial compression test along the y axis (perpendicular to the bed joints), under displacement control condition, is performed on the samples. Cracking and crushing occurred in the sample No. 3 that is illustrated in Figure 6. Compression behavior of the sample is found from universal testing machine is shown in Figure 7.

In order to obtain the tension regime of the

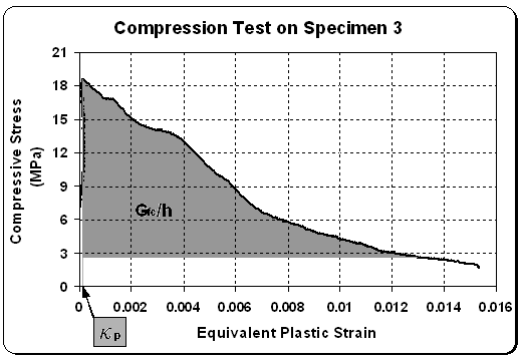

Fig. 7 Behavior of masonry sample No.3 under compression

Fig. 8 Failure development in masonry sample No.3 at last loading step

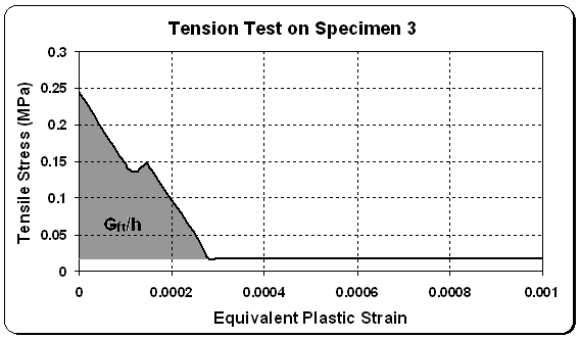

Fig. 9 Behavior of masonry sample No.3 under tension

Rankin-Hill yield surface, three similar samples, without any caps at both ends, are constructed in IIEES laboratory similar to the compressive samples. The masonry samples have dimensions of 108x230x357, 105x225x361 and 108x230x357, all in mm. The uniaxial tension test along the y axis (perpendicular to the bed joints) is performed on the samples, under displacement control condition. The load is applied by steel plates attached to the top and bottom of the samples by special glue (Sikadur 32). As expected, tension failure is occurred due to relatively low tensile bond strength between the bed joint and the brick unit (Figure 8). Tensile behavior of the sample No.3 which is determined from universal testing machine is shown in Figure 9.

Table 1 Elastic properties of URM walls

E(MPa)	▪
2500.00	0.15

After carrying out experimental studies on masonry samples, the material properties obtained by averaging the experimental results. The isotropic material properties of masonry wall, in linear elastic range, are shown in Table 1. The modulus of elasticity is defined as a secant modulus at service load conditions in compression tests, i.e. at 1/3 of maximum vertical load [11]. The yield criterion for orthotropic material behavior used in the present study combines a Hill–type criterion for compression and a Rankine–type criterion for tension with low orthotropic factor. Then inelastic properties of masonry wall are shown in Tables 2 and 3. All of the parameters shown in bellow mentioned tables are obtained from experimental studies except ν , α , β and γ . These parameters are assumed as typical values in masonry structures.

4. Material Properties of Interface

In accordance with Iranian Standard No. 2800, the RC members and the masonry panel should

Table 2 Inelastic properties of URM walls (tension is governing)

f_{tx} (MPa)	f_{ty} (MPa)	▪	G_{ftx} (Nmm/mm^2)	G_{fty} (Nmm/mm^2)
0.14618	0.14618	1.00	0.01575	0.01575

Table 3 Inelastic properties of URM walls (compression is governing)

f_{mx} (MPa)	f_{my} (MPa)	▪	▪	G_{fcx} (Nmm/mm^2)	G_{fcy} (Nmm/mm^2)	▪$_p$
16.3768	16.3768	-1.00	3.00	29.3390	29.3390	0.000645

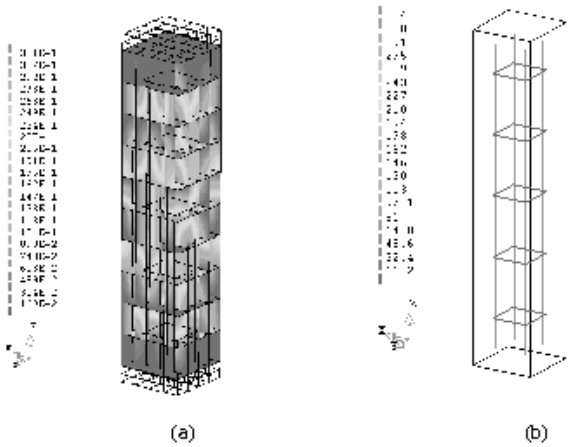

Fig. 10 RC member in tension at last loading step: (a) crack pattern form, (b) stress in longitudinal reinforcements

be joined together in confined masonry buildings. Here, the material properties of interface element are calculated according to experimental results. A plasticity based model is adopted for modeling the interface, which has zero width, between the interior rim of RC members and the exterior perimeter of masonry panel. This model consists of non-associated Coulomb friction model with tension cut-off mode. Values of the normal interface stiffness (k_n) and the shear interface stiffness (k_s), within linear elastic range, are given in Table 4. For concrete interface modeling, the nonlinear material properties are obtained based on the specified compressive strength of concrete (f'_c). The average value of the (f'_c) is determined as 28 MPa, after carrying out compression test on 9 standard concrete specimen. The nonlinear interface properties consist of tensile strength (f_t), cohesion (c) and friction angle (ϕ) which are calculated according to requirements of ACI 318-02 [12] and they are presented in Table 5. Dilatancy angle, shown by ψ, is taken as constant and set to zero. This means that the RC members can slide over the masonry panel without developing any vertical displacement.

5. Material Properties of RC Members

Material properties of RC members are evaluated based on analytical studies. Meanwhile, due to lack of having a reliable plasticity model for under-reinforced RC members, a simple Rankine plasticity criterion is used. To calibrate the RC bond-beams and tie-columns model, a 3-dimensional RC member with dimensions of 1000mmx210mm x210mm is modeled by DIANA. The direct tensile load is applied by steel plates attached to the top and bottom of the RC member. The concrete is modeled by 20 nodded isoparametric solid elements CHX60 [6]. For modeling the concrete behavior, modified Maekawa concrete model is used. Crack model is directly related to the total strain crack model for the tensile regime in modified Maekawa model. In this modified model, total strain rotating crack with exponential softening in tension is employed. The attractive point of the selected model is that it is defined by engineering parameters such as the tensile and compressive strength and the fracture energy. Mode-I of fracture energy (in tensile regime) is obtained from the following relation [13]:

$$G_F^I = \alpha_F . (\frac{f'_c}{10})^{0.7} \quad (1)$$

Where α_F=coefficient which depends on the maximum aggregate size, $d_{\max}$ (α_F=0.058

Table 4 Elastic properties of interface

k_n(N/mm³)	k_s(N/mm³)
2800	1200

Table 5 Inelastic properties of interface

c(MPa)	tan•	tan•	f_t(MPa)
0.88	0.065	0.00	2.94

Table 6 Elastic properties of concrete

E(MPa)	•
26458	0.2

Table 7 Inelastic properties of concrete

f_c(MPa)	f_t(MPa)	G_f^I(N.mm/mm²)	h(mm)
28.00	2.94	0.12	65

N.mm/mm² for d_{max}=32 mm), and (f'_c)= mean cylinder strength in MPa. Within linear elastic range, the concrete Young's modulus (E) and the concrete Poisson's ratio (ν) are calculated and presented in Table 6. The concrete nonlinear properties comprise of shear retention factor β, compressive strength (f'_c), tensile strength (f_t), mode-I of fracture energy (G_f^I) and a crack band width (h) which can be determined and shown in Table 7.

The steel reinforcement bars, bonded in the concrete, consist of 4 longitudinal reinforcement of 10 mm diameter; 5 transverse reinforcement of 6 mm diameter and are placed at 110 mm and 200 mm center to center, respectively. Von Mises plasticity without hardening is used for longitudinal reinforcement bars. Also, Young's modulus equals to E= 2.1x10^5 MPa and steel yield stress equals to σ_y=340 MPa. On the other hand, the same plasticity model is applied for transverse reinforcement bars but the yield stress equals to σ_y=220 MPa.

In the nonlinear analysis, the tensile displacement load in the center of the top steel plate in the +Z direction is applied when the bottom steel plate is suppressed the translation along the X, Y and Z directions. The loading size determined automatically at every loading step with maximum size of 0.000001 built in DIANA. The crack pattern form at last loading step is illustrated in Figure 10-a. The normal crack strain ε_{nn}^{cr} present as contour levels shows that around the midheight of the RC member the crack strains increased considerably. The stress in longitudinal reinforcements in Z direction is illustrated in Figure 10-b. This Figure represents that all of the longitudinal reinforcements yielded at last loading step.

In this study, the RC element is under-reinforced. The tensile capacity of the reinforced concrete (before cracking) is greater than the tensile strength of the longitudinal reinforcing bars. Figure 11 shows that stress-strain curve in tension has an initial peak representing the cracking strength of the reinforced concrete. This followed by a decline in strength to the yield strength of the longitudinal reinforcements. This Figure shows that all of the longitudinal reinforcement bars yielded after the concrete had cracked. Therefore the Rankine yield stress value of the RC members is approximately equal to 3.00 MPa.

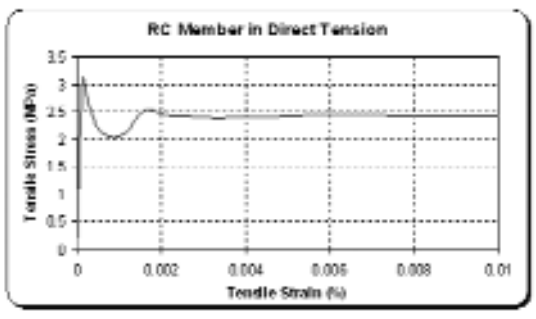

Fig 11 Tensile stress-strain curve for RC member

6. Validation of FE models

Validation of FE models was performed by another study by the same authors [5]. For this purpose, experimental and numerical studies are carried out on a half scale typical confined masonry wall by the same load pattern. Two identical specimens of the wall are tested under static monotonic lateral loading. The Iranian

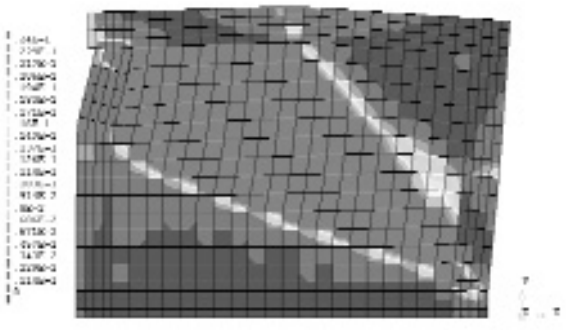

Fig 12 Contour form of cracks at last loading step

Fig 13 Separation of plaster due to crack formation in specimen B at last loading step

seismic code provisions are used for making both test specimens (A and B). Also the assumptions used in this study and the validation study are all the same. Based on the experimental and numerical results, the obtained crack pattern and capacity curves are compared and good agreement is achieved. In respect to cracking pattern (Figures 12 & 13), the following results can be presented:

- Diagonal cracking of the masonry panel is found.
- Cracking in masonry panel tends to concentrate in a wide shear band, going from one corner of the specimen to the other. The shear band width near the horizontal applied load is larger than the other end.
- The shear band extended to the intersections of the RC members. This means that the cracking initially occurred in masonry panel and then penetrated to the intersections of the RC members.
- The cracks appeared at the upper bond–beam and the left hand-side tie–column of the wall panel.
- The crack formation and interpenetration did not happen at the interface element.

The comparison between numerical and experimental capacity curves shows that (Figure 14):

- Three capacity curves have the same trend.
- The maximum lateral strength has almost the same values.
- The initial stiffness of analytical capacity curve is located between two results obtained by experimental study.
- From a drift angle of approximately 0.3% on, the numerical and experimental load-drift angle diagrams are almost parallel.

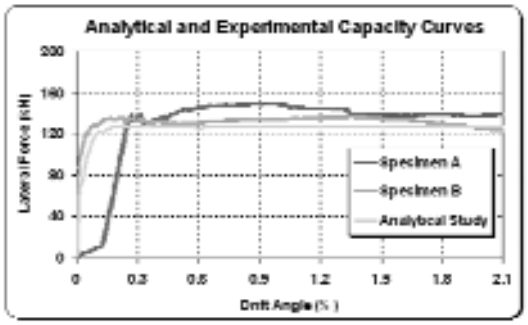

Fig 14 Comparison between capacity curves

7. Nonlinear Analysis

A pushover analysis is performed to obtain the cracking pattern, distribution of the maximum and minimum principal stresses and the force–deformation curve (capacity curve). The analysis type is physically nonlinear. The loading size determined automatically at every loading step with maximum size of 0.00001 built in DIANA. For pushover analysis of a confined masonry wall, a monotonic lateral load should apply on the top of model based on the ATC-40 requirements [14]. This guideline does not recommend any other load pattern to apply on one story buildings. The iteration method used in this study is regular Newton – Raphson. The augmented lateral displacement load is applied at the upper RC bond – beam from left to right after the gravity load analysis is performed. The gravity load is due to self weight of the confined masonry walls without any additional vertical loads.

8. Nonlinear Analysis Results

8.1 Crack Formation and Maximum Principal Stress Distribution

Crack formation is illustrated in Figures 15, 16, 17 and 18. This Figures present contour plot form in the **P** wall and the **P+O** wall respectively. All of the below mentioned Figures illustrate crack formation and the normal crack strain present as contour levels on the left hand side of them.

These Figures give contour plot form of the crack in deformed meshes on the masonry panel and on the RC members respectively. In the masonry panel cracks are plotted normal to the tensile principal plastic strain directions. Figures 16&18 can not be able to show the crack pattern on the RC member because it displays of plastic strain contours (as crack pattern) used in masonry analysis only. But Figures 15&17 show the crack

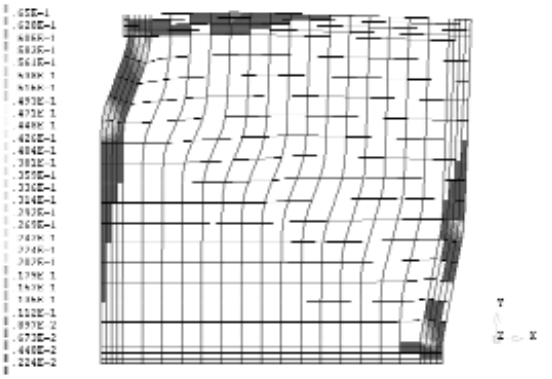

Fig 15 Crack pattern on bond-beams and tie-columns at last loading step

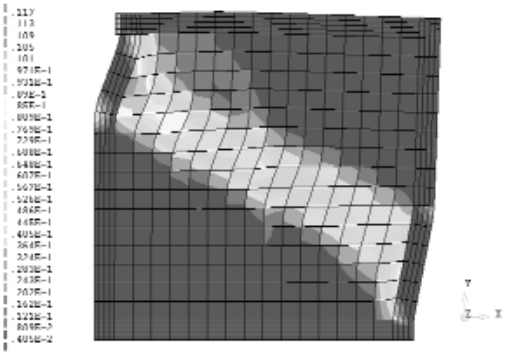

Fig 16 Crack pattern on masonry panel at last loading step

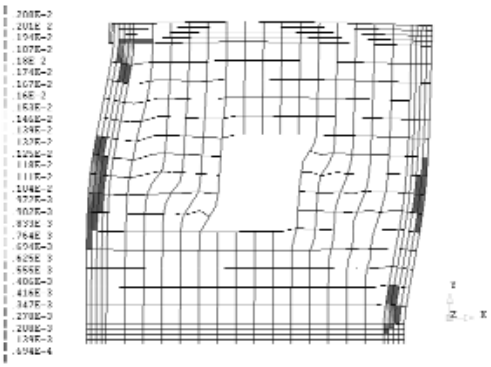

Fig 17 Crack pattern on bond-beams and tie-columns at last loading step

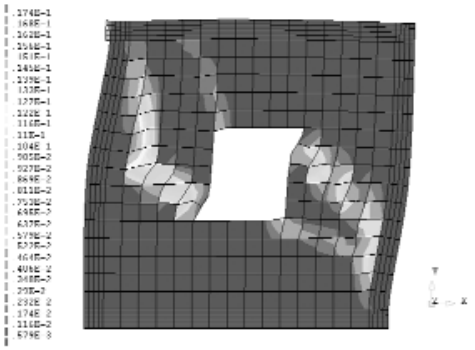

Fig 18 Crack pattern on masonry panel at last loading step

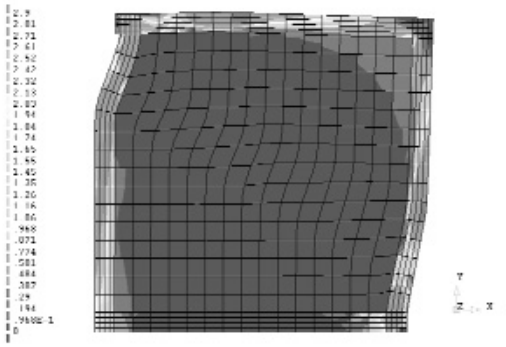

Fig 19 Maximum principal stress contours of the **P** wall at last loading step (Tensile stresses are positive)

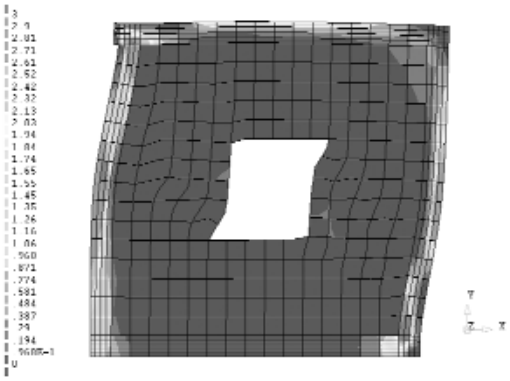

Fig 20 Maximum principal stress contours of the **P+O** wall at last loading step (Tensile stresses are positive)

pattern on the RC member as "smeared crack" model.

In the case of the **P** wall, the displays show clearly that cracks appear at the upper bond – beam and tie – columns at left and right hand side of the wall panel. Also the crack formation will happen in the masonry panel as a diagonal crack. But in the case of the **P+O** wall, the crack formation becomes visible at RC members and every corners of the opening. This condition proves that the opening corners may be vulnerable. Also cracking can not be observed in interface elements in both walls.

As shown in Figures 19 & 20, maximum principal stress distribution in some areas of masonry panel is greater than and at the last loading step. Therefore failure in masonry panel is governed by the tension regime and the stress values are setting on softening branch of stress-strain diagram. The position of the stress point on softening branch of stress-strain relationship can be used as a measure to compare with a

predefined maximum value. This can lead to quantify the level of masonry damage for different regions at different load steps.

The cracked regions in RC members are coincided with the largest value of maximum positive principal stress contours at the same locations (see Figures 15&19 and also Figures17&20). So, the cracked regions in RC frames suffered tension stresses higher than the Rankine yield stress 3.00 MPa.

8.2 Minimum Principal Stress Contours

In Figures 21 and 22, minimum principal stress contours are shown on deformed meshes. In the **P** wall, Figure 21 clearly shows the compressive inclined strut region in the masonry panel. They are created the stress zones and therefore, the internal forces flow in them. In the **P+O** wall, the inclined strut action may be weakened. Then the strength of the wall diminishes and at the end of loading the **P+O** wall is collapsed.

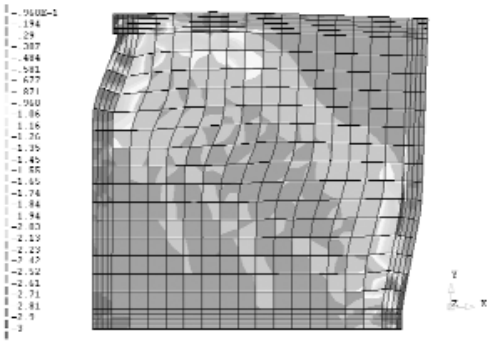

Fig 21 Minimum principal stress contours of the **P** wall at last loading step (Compressive stresses are negative)

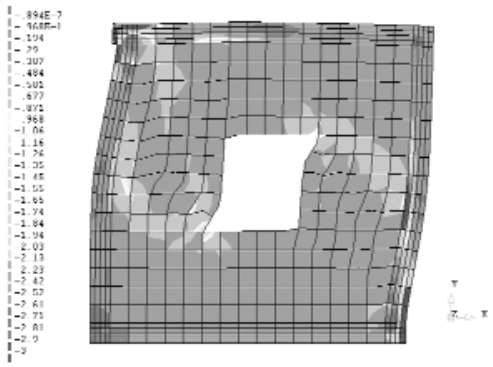

Fig 22 Minimum principal stress contours of the **P+O** wall at last loading step (Compressive stresses are negative)

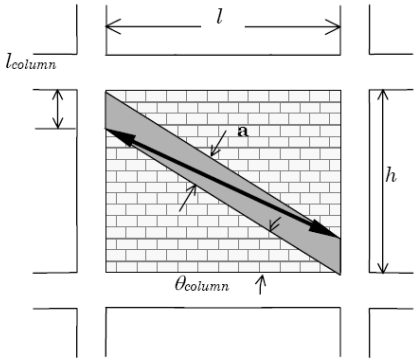

Fig 23 The equivalent masonry strut placement [17]

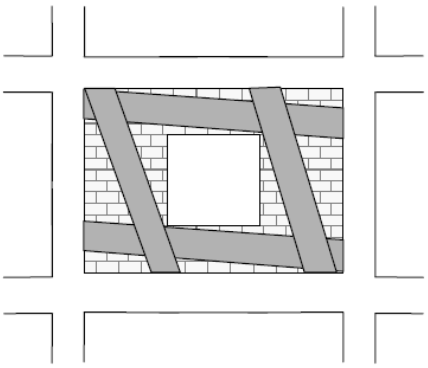

Fig 24 The possible struts placement in the perforated infill panel [17]

By simplification in infilled frame analysis, the masonry infill can be replaced by an equivalent compressive masonry strut as shown in Figure 23. The evaluation of the equivalent compressive masonry strut width, a, presented by Paulay and Priestley [15] who have assumed constant values for the strut width, a, between 12.5 to 25 percent of the diagonal dimension of the infill. In this study, the minimum principal stress contours of the **P** wall shows that about 40 percent of the diagonal dimension of the masonry panel is contributing for the strut width.

On the other hand, the perforated infill panel may be replaced by diagonally concentric equivalent struts used to analytical model as shown in Figure 24. This stress fields with multiple compression struts was proposed by Hamburger [16]. In accordance with FEMA 356, theoretical work and experimental data for determining multiple struts placement and struts properties are not sufficient to establish reliable guidelines. As shown in Figure 22, the minimum

principal stress contours of the **P+O** wall do not show these stress fields.

On the basis of literature review, infilled frames have compressive struts but their strut placements and their strut shapes are not sufficient to establish reliable guidelines in confined masonry walls. Therefore use of infilled frame approaches in confined masonry walls requires precaution and engineering judgment.

8.3 Capacity Curves

The capacity curves for the **P** wall and the **P+O** wall are illustrated in Figures 25 and 26. The capacity curve is calculated by DIANA at the node that lateral displacement load is applied on it. This node is coincided on the center of the rigid plate that glued on the upper-left of the confined masonry wall.

Stiffness of the **P** wall and the **P+O** wall can be estimated based on the developed bilinear load-deflection curves. The initial stiffness of the **P** and the **P+O** is about 160kN/mm and 95kN/mm respectively. In Figure 25, the **P** wall is carrying a peak lateral force of 83500N and a peak drift angle equal to 1.17%. In the Figure 26, before collapse point, the **P+O** wall is carrying a peak lateral force of 53800N and a peak drift angle equal to 0.11%. Large differences between them are observed. The load-deflection curves (capacity curves) show that the ratio of initial stiffness of the **P+O** wall to the **P** wall is about 0.59 and the ratio of peak lateral loads in the **P+O** wall to the **P** wall is about 0.64. Also, ultimate deformation capacity of the **P+O** wall is about 1/10 ultimate deformation capacity of the **P** wall. On the other hand, Iranian Seismic Code provisions emphasizes on providing the confining elements around large openings, those with a dimension larger than 2.5 meters. Based on this study, it is revealed that this requirement does not seem conservative and must be revised based on further researches.

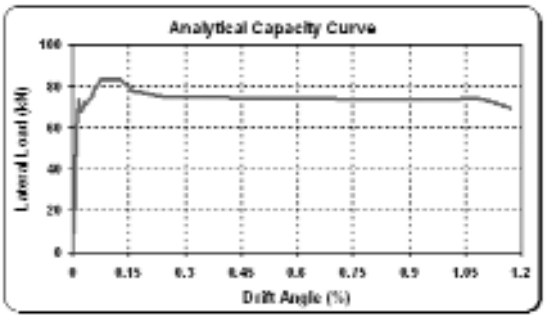

Fig 25 Capacity curve of the **P** wall

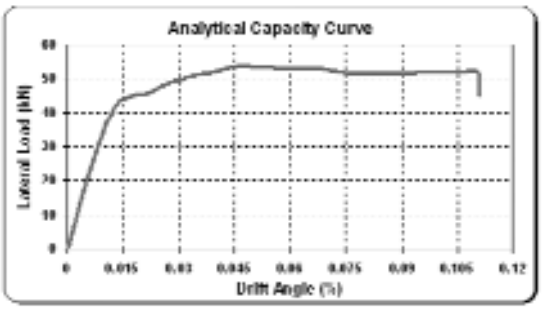

Fig 26 Capacity curve of the **P+O** wall

9. Conclusions

This study is carried out in order to evaluate the crack pattern; maximum and minimum principal stress contours and capacity curves for confined masonry walls with opening **(P+O)** and confined masonry walls without opening **(P)**. Also, a further investigation is needed for estimating capacity of confined masonry walls without and with opening for different orientations and sizes either analytically and/or experimentally.

Based on the results, the following conclusions are presented:

1- In the case of the **P** wall, cracks appear at the upper bond–beam and tie–columns at left and right hand side of the wall panel. Also, the crack formation occurs within the masonry panel along diagonal direction. But in the case of the **P+O** wall, the crack formation is seen not only at RC members but also at every corners of the opening. This illustrates that the opening corners might be vulnerable.

2. In infilled frames with and without opening, the compressive strut model can be assumed as inclined bands. But, this compressive strut in confined masonry wall is different. The difference is in the compressive strut orientation and shape, mainly due to the cohesion between

the RC members and the masonry panel.

3. The load-deflection curves (capacity curves) show that the ratio of initial stiffness of the **P+O** wall to the **P** wall is about 0.59 and the ratio of peak lateral loads in the **P+O** wall to the **P** wall is about 0.64. Also, ultimate deformation capacity of the **P+O** wall is about 1/10 ultimate deformation capacity of the **P** wall.

4. Iranian Seismic Code emphasizes on providing the confining elements around large openings only. Based on this study, it is revealed that this requirement must be revised to include the medium sizes of openings as well.

References

[1]. EERI: 2004, Confined Masonry Construction, World Housing Encyclopedia Report.

[2]. Building and Housing Research Center: 2005, Iranian Code of Practice for Seismic Resistant Design of Buildings, Standard No.2800 – 05, Third Edition. (In Persian)

[3]. NTC-M 2004, Normas Tecnicas Complementarias para Diseno y Construccion de Estructuras de Mamposteria, Gobierno del Distrito Federal, 47 pp.(In Spanish)

[4]. Alcocer, S.M., Arias, J.G., Flores, L.E: 2004, Some developments on performance – based seismic design of masonry structures, Proceedings of an International Workshop on Performance – Based Seismic Design Concepts and Implementation, pp. 233-244.

[5]. Pourazin, Kh., Eshghi, S.:2009, In-Plane Behavior of a Confined Masonry Wall, The Masonry Society Journal.(Accepted for publication)

[6]. Delft, TNO Building and Construction Research: 2005, DIANA Finite Element Analysis, User's Manual – Element Library.

[7]. Mohammadi, S.: 2003, Discontinuum Mechanics Using Finite and Discrete Elements, WIT press.

[8]. Lourenco, P.B.: 1996, Computational Strategies for Masonry Structures, Ph.D. thesis, Delft University of Technology, Delft, Netherlands.

[9]. Page A.W.: 1981, The Biaxial Compressive Strength of Brick Masonry, Proc. Intsn .Civ. Engrs., Part 2, 71 , pp. 893-906.

[10]. Page A.W.: 1983, The Strength of Brick Masonry Under Biaxial Compression – Tension, Int. J. Masonry Constr., 3(1), pp. 26-31.

[11]. Eurocode 6: 1996, Design of Masonry Structures, DD ENV 1996-1-1:1996, Part 1-1. General Rules for Buildings – Rules for Reinforced and Unreinforced Masonry.

[12]. ACI 318-02: 2002, Building Code Requirements for Structural Concrete, Reported by ACI committee 318.

[13]. CEB – FIP: 1993, CEB – FIP Model Code 1990, Comite Euro International du Beton.

[14]. Applied Technology Council: 1996, Seismic evaluation and retrofit of concrete buildings: Vol. 1&2, ATC 40, Redwood City.

[15]. Paulay, T., Priestley, M.J.N.: 1992, Seismic Design of Reinforced Concrete and Masonry Buildings, John Wiley & Sons.

[16]. Hamburger, R.O.:1993, Methodology for Seismic Capacity Evaluation of Steel - Frame Buildings with Infill Unreinforced Masonry, Proceedings of 1993 National Earthquake Conference, Centeral U.S. Earthquake Consortium, Vol. , pp. 173 – 191, Memphis, Tennessee.

[17]. Al-Chaar, Gh.: 2002, Evaluating Strength and Stiffness of Unreinforced Masonry Infill Structures, U.S. Army Corps of Engineers, ERDC/CERL TR-02-1, Construction Engineering Research Laboratory.